Mon. Not. R. Astron. Soc. **000**, 1–11 (2009) Printed 8 June 2009 (MN LATEX style file v2.2)

Spectral variability of ultraluminous X-ray sources

Jari J. E. Kajava⋆ and Juri Poutanen⋆
Department of Physical Sciences, Astronomy division, P.O.Box 3000, 90014 University of Oulu, Finland

arXiv:0906.1485v1 [astro-ph.HE] 8 Jun 2009

Accepted 2009 June 07. Received 2009 June 07; in original form 2008 November 21

ABSTRACT
We study spectral variability of 11 ultraluminous X-ray sources (ULX) using archived *XMM-Newton* and *Chandra* observations. We use three models to describe the observed spectra: a power-law, a multi-colour disc (MCD) and a combination of these two models. We find that 7 ULXs show a correlation between the luminosity $L_{\rm X}$ and the photon index Γ. Furthermore, 4 out of these 7 ULXs also show spectral pivoting in the observed energy band. We also find that two ULXs show an $L_{\rm X}-\Gamma$ anti-correlation. The spectra of 4 ULXs in the sample can be adequately fitted with a MCD model. We compare these sources to known black hole binaries (BHB) and find that they follow similar paths in their luminosity-temperature diagrams. Finally we show that the 'soft excess' reported for many of these ULXs at ~ 0.2 keV seems to roughly follow a trend $L_{\rm soft}\propto T^{-3.5}$ when modelled with a power-law plus a 'cool' MCD model. This is contrary to the $L\propto T^4$ relation that is expected from theory and what is seen for many accreting BHBs. The observed trend could instead arise from disc emission beamed by an outflowing wind around a ~ 10 solar mass black hole.

Key words: accretion, accretion discs – black hole physics – galaxies: individual: NGC 253, NGC 1313, PGC 13826, PGC 23324, PGC 28757, NGC 5204, NGC 5408, NGC 6946 – X-rays: binaries – X-rays: galaxies.

1 INTRODUCTION

Ultraluminous X-ray sources (ULX) are point like, non-nuclear (not an active galactic nucleus, AGN) objects with X-ray luminosities exceeding the Eddington limit for stellar mass black holes (StMBH), $L_{\rm Edd}\approx 1.3\times10^{39}(M/10{\rm M}_\odot)\,{\rm erg\,s^{-1}}$. Many ULXs have been identified as accreting black holes because of their short- and long-term variability (Miller & Colbert 2004, and references therein). More than 300 ULXs have been discovered in nearby galaxies (Liu 2008) and all types of galaxies have ULXs (Mushotzky 2006). Although they were discovered with the *Einstein* mission almost thirty years ago (see Fabbiano 1989, for review), the nature of these sources is not yet well understood.

Assuming that ULXs are isotropic emitters, the most luminous source M82 X-1 has a luminosity of $L_{\rm X}\sim10^{41}\,{\rm erg\,s^{-1}}$ (Patruno et al. 2006). Therefore, for such a high luminosity ULX the accreting black hole should be an intermediate-mass black hole (IMBH) with $M\gtrsim1000{\rm M}_\odot$ not to exceed the Eddington limit. One argument used to support this idea is the presence of a ~ 0.2 keV 'soft excess' in the spectra of several luminous ULXs (Kaaret et al. 2003; Miller et al. 2003), which could be interpreted as a signature of a 'cool' accretion disc around an IMBH. It is also possible, however, that this excess arises from the emission at a large distance from the central source (King et al. 2001; Poutanen et al. 2007) or, maybe, is an artifact of a complicated absorber or emission from some thermal plasma surrounding the source (Gonçalves & Soria 2006). Another argument used in favour of the IMBH interpretation is the detection of low-frequency quasi-periodic oscillations (QPO) from ULXs in M82, Holmberg IX and NGC 5408 (Strohmayer & Mushotzky 2003; Dewangan et al. 2006; Strohmayer et al. 2007). However, similar QPO frequencies have been also detected from Cyg X-1 (Vikhlinin et al. 1994), which is certainly not an IMBH.

There are also several arguments against the hypothesis that ULXs are powered by accretion onto IMBHs. The main issue is the formation of such massive objects in 'normal' stellar evolution. Black holes of masses greater than $80{\rm M}_\odot$ are not expected to form even in the lowest metallicity environments and at solar metallicities the upper limit is about $15{\rm M}_\odot$ (Belczynski et al. 2009). Furthermore, about 30 per cent of ULXs are associated with star formation regions (Mushotzky 2006) and a small number of them have been associated with young stellar counterparts (Mushotzky 2006; Roberts et al. 2008). These facts can be naturally explained if ULXs are powered by accretion onto StMBHs.

There are numerous models put forward on how the luminosity of a StMBH can exceed its Eddington limit. Truly super-Eddington models include the advective slim disc models (Jaroszyński et al. 1980; Abramowicz et al. 1988; Kawaguchi 2003), which have been successfully used to describe some ULX spectra (Vierdayanti et al. 2006). Accretion discs with strong outflows (Shakura & Sunyaev 1973; King et al. 2001; King & Puchnarewicz 2002; Poutanen et al. 2007) can also explain the high luminosities of ULXs. Other plausible scenarios involving StMBHs that can produce the high observed luminosities in-

⋆ E-mail: jari.kajava@oulu.fi (JJEK), juri.poutanen@oulu.fi (JP)

Table 1. Observation log

ULX name	Alternate names	Coordinate J2000	Distance[a] Mpc	Observation IDs *XMM-Newton*	*Chandra*
NGC 253 X-2	NGC 253 PSX-2 NGC 253 ULX2 NGC253 XMM1	00:47:33.0 −25:17:49	3.0	0110900101 0125960101 0125960201 0152020101 0304850901 0304851001 0304851201 0304851101	790
NGC 253 X-4	NGC 253 PSX-7 NGC253 XMM3	00:47:35.3 −25:15:12	3.0	0110900101 0125960101 0152020101 0304850901 0304851001	790 3931
NGC 253 X-9	NGC 253 PSX-5 NGC253 XMM2	00:47:22.6 −25:20:51	3.0	0110900101 0125960101 0152020101 0304850901 0304851001 0304851201	3931
NGC 1313 ULX-1	NGC1313 XMM1 IXO 7	03:18:19.8 −66:29:10	3.7	0106860101 0150280301 0150280401 0150280601 0150281101 0205230201 0205230301 0205230401 0205230501 0205230601 0405090101	
NGC 1313 ULX-2	NGC1313 XMM3 IXO 8	03:18:22.0 −66:36:04	3.7	0106860101 0150280101 0150280301 0150280401 0150280501 0150280601 0150281101 0205230201 0205230301 0205230401 0205230501 0205230601 0301860101 0405090101	
IC 342 X-6	IC 342 ULX1 IXO 22	03:45:55.7 +68:04:55	3.9	0093640901 0206890101 0206890201 0206890401	2916 2917
HoII ULX-1	IXO 31	08:19:29.0 +70:42:19	3.39	0112520601 0112520701 0112520901 0200470101	
HoIX ULX-1	NGC 3031 ULX2 IXO 34	09:57:54.1 +69:03:47	3.42	0112521001 0112521101 0200980101	3786 3787 3788
NGC 5204 ULX-1	NGC5204 XMM1 IXO 77	13:29:38.6 +58:25:06	4.3	0142770101 0142770301 0150650301 0405690101 0405690201 0405690501	3933
NGC 5408 ULX-1	NGC5408 XMM1	14:03:19.6 −41:23:00	4.8	0112290501 0112290601 0112290701 0112291201 0302900101	
NGC 6946 X-6	NGC 6946 ULX3	20:35:00.7 +60:11:31	5.5	0200670301 0401360301	1043 4404 4631 4632 4633

[a] Distance estimates are from Liu & Bregman (2005) except for HoII ULX-1 and NGC 5408 ULX-1, where the distances are taken from Karachentsev et al. (2002) and Liu & Mirabel (2005), respectively.

clude the photon bubble model (Arons 1992; Begelman 2001) and beaming of radiation by a relativistic jet (Körding et al. 2002; Freeland et al. 2006). Strong beaming, however, can be ruled out in some cases by observations of photo-ionised nebulae surrounding the ULXs because the observed line properties require luminosities comparable to the observed X-ray luminosities (Pakull & Mirioni 2003; Kaaret et al. 2004; Abolmasov et al. 2007; Kaaret & Corbel 2009).

Because of the limited observing band of the current X-ray observatories capable of detecting ULXs ($\sim 0.2-10$ keV), it is not surprising that many of the models mentioned above have been successfully used to model the observed spectra of some particular ULX. This is mainly because many previous studies have been concentrated only on modelling single observations of individual ULXs (e.g. Feng & Kaaret 2005; Winter et al. 2006; Stobbart et al. 2006). The lack of multi epoch observations can lead to misinterpretation of the physical meaning of the derived spectral parameters. By studying the spectral variability of ULXs, we hope to learn more about the physical nature of the specific spectral components by comparing their variations to expectations from theoretical models. Some previous works have studied spectral variability of ULXs (Fabbiano et al. 2003; Dewangan et al. 2004; Feng & Kaaret 2006a,b; Roberts et al. 2006; Berghea et al. 2008), but the samples of ULX with multiple observations have been small.[1] Interestingly, the study by Feng & Kaaret (2006b) showed that the two ULXs in NGC 1313 galaxy have different types of spectral variability. Their subsequent study (Feng & Kaaret 2007) also showed that the soft excess in NGC 1313 ULX-2 did not follow the $L \propto T^4$ relation that is expected from theory when modelled with a multi-colour disc (MCD). Therefore, in order to study the spectral variability of ULXs in better detail, we have selected a sample of 11 ULXs that have been observed multiple times with *XMM-Newton* and *Chandra*. In this paper, we present the results of spectral analysis of these data sets.

2 OBSERVATIONS AND DATA REDUCTION

We searched the data archives for high S/N *XMM-Newton* and *Chandra* observations of ULXs that have been observed multiple times. We also required that the observations were not effected by photon pile-up. There were 11 sources that met the requirements: NGC 253 X-2, NGC 253 X-4, NGC 253 X-9, IC 342 X-6, NGC 1313 ULX-1, NGC 1313 ULX-2, Holmberg II ULX-1, Holmberg IX ULX-1, NGC 5204 ULX-1, NGC 5408 ULX-1 and NGC 6946

[1] Note a recent paper by Feng & Kaaret (2009), who consider a large sample of ULXs.

X-6 (see Table 1). In the cases where sources have multiple names, we followed the naming convention of Liu & Bregman (2005).

XMM-Newton data reduction was done using the SAS version 7.1.0. In order to produce a homogeneously calibrated data set, we processed all the observations using the observation data files with the latest calibration files as of March 2008. The reduction was done according to the User's guide to the *XMM-Newton* Science Analysis System.[2] Specifically, we used the event selections "FLAG==0 && PATTERN<=4" and "#XMMEA_EM && PATTERN<=12" for the EPIC-pn and EPIC-mos instruments, respectively. *Chandra* observations were reduced using the CIAO 4.0.1 software. We processed all the observations with calibration files from CALDB 3.4.3 following the *Chandra* science threads.[3]

We used circular source extraction regions of varying radii (between 20" to 40" for *XMM-Newton* and 4" to 12" for *Chandra*). Close-by source free regions were used as a background.[4] The resulting background subtracted spectral data were binned to require at least 20 counts per bin to ensure adequate statistics for the XSPEC spectral fitting. To ensure the best possible spectral quality, the time periods of high background were eliminated from the data for both *XMM-Newton* and *Chandra* observations. In the case of *XMM-Newton* the exclusion was done by removing the time periods where the 10−12 keV full field count rate was above 0.4 cts s^{-1} and 0.35 cts s^{-1} for EPIC pn and mos, respectively. For *Chandra*, we used the ANALYZE_LTCRV.SL script on a source free event file to remove the high background periods.

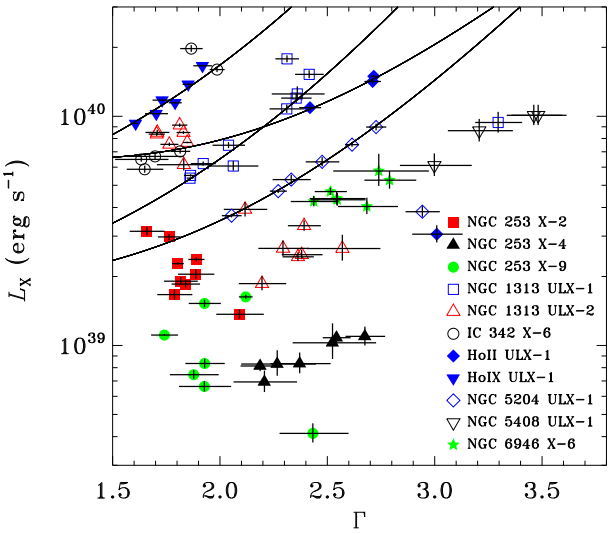


Figure 1. The intrinsic 0.4−10 keV band luminosity versus the photon index obtained from the POWERLAW model fits. Different observations of a given object showing spectral pivoting in the observed band are connected by a theoretical curve (1). Some sources show correlation, but no spectral pivoting and some other even show anti-correlation. NGC 1313 ULX-1, Holmberg II ULX-1, Holmberg IX ULX-1, NGC 5204 ULX-1 show $L_{\rm X}-\Gamma$ correlation *with* spectral pivoting in the observed band. NGC 253 X-4, IC 342 X-6 and NGC 5408 ULX-1 show $L_{\rm X}-\Gamma$ correlation *without* spectral pivoting, and NGC 253 X-2 and NGC 1313 ULX-2 are $L_{\rm X}-\Gamma$ anti-correlated sources. NGC 253 X-9 shows no $L_{\rm X}-\Gamma$ correlation and NGC 6946 X-6 is not variable enough to make firm conclusions.

3 SPECTRAL ANALYSIS AND RESULTS

We used three models to describe the observed spectra: a POWERLAW, a MCD (DISKBB model in XSPEC) and a combination of these two models. The effect of the interstellar medium was taken into account with the WABS model in XSPEC. The hydrogen column density was let as a free parameter, but was required to have at least the Galactic value (Dickey & Lockman 1990). In some cases, none of these simple models gave statistically acceptable fits to the data. In most of these cases, the fits could have been improved by adding more model components like gaussians at $\lesssim 1$ keV (NGC 5204 ULX-1, OBSID 3933, see Roberts et al. (2006); NGC 5408 ULX-1, OBSID 0302900101) or by changing metal abundances of the absorber (HoII ULX-1, see Goad et al. (2006)). We checked that our best fitting parameters did not change significantly by adding these components, so we decided to ignore these facts, because we wanted to keep our models as simple as possible.

We fit the spectra in the 0.4−10 keV band (or up to energies which are not noise dominated). XMM-Newton provides spectral coverage down to ~ 0.2 keV, but we decided to restrict our fitting range to 0.4 keV because of the known calibration uncertainties below this value.[5] All the parameter errors in the following figures are given at the 90 per cent confidence level. The errors for the fluxes were computed using the CFLUX convolution model in XSPEC. In the case of the POWERLAW model, the luminosities were calculated for the 0.4−10 keV band. The MCD component luminosities are bolometric.

3.1 Power-law type ULXs and the $L_{\rm X}-\Gamma$ correlation

A simple absorbed POWERLAW model provides a good fit for most of the observations in our sample (see Table A1). We find a correlation between the luminosity and the photon index (hereafter $L_{\rm X}-\Gamma$ correlation) for most of the ULXs, see Fig. 1. Similar correlations were also observed for NGC 1313 ULX-1 (Feng & Kaaret 2006b) and Antennae X-11 (Feng & Kaaret 2006a). The ULXs with the $L_{\rm X}-\Gamma$ correlation are NGC 253 X-4, IC 342 X-6, NGC 1313 ULX-1, Holmberg II ULX-1, Holmberg IX ULX-1, NGC 5204 ULX-1 and NGC 5408 ULX-1. In contrast, two ULXs of the sample, NGC 253 X-2 and NGC 1313 ULX-2, show an anti-correlation between the luminosity and Γ (see Fig. 1 and Feng & Kaaret 2006a,b, for comparison). We also find that the luminosity of NGC 253 X-9 is clearly not correlated with Γ and that NGC 6946 X-6 is not significantly variable to make firm conclusions.

For NGC 1313 ULX-1, Holmberg IX ULX-1 and NGC 5204 ULX-1, the modelled absorption column $N_{\rm H}$ is also correlated with Γ (see also fig. 1 in Feng & Kaaret 2009, for NGC 5204 ULX-1). If this correlation has no physical origin, then the luminosities of the softest spectra would be 'artificially boosted'. To evaluate this effect on the derived *intrinsic* luminosities, we fixed the absorption columns to their mean values, and fitted the data again. This lead to somewhat worse fits for the cases where the best fitting absorption columns differ most from the mean, but the $L_{\rm X}-\Gamma$ correlations remained. Also, the observed (i.e. absorbed) luminosities $L_{\rm abs}$ are correlated with Γ, but the $N_{\rm H}-\Gamma$ dependence leads to a 'shallower'

[2] Guide is available at http://xmm.esac.esa.int/external/xmm_user_support/documentation/sas_usg/USG.pdf.
[3] Threads are available at http://cxc.harvard.edu/ciao/threads/index.html.
[4] In the case of *XMM-Newton*, the background region was chosen from the same EPIC-pn CCD chip as the source.
[5] See EPIC status of calibration and data analysis XMM-SOC-CAL-TN-0018.

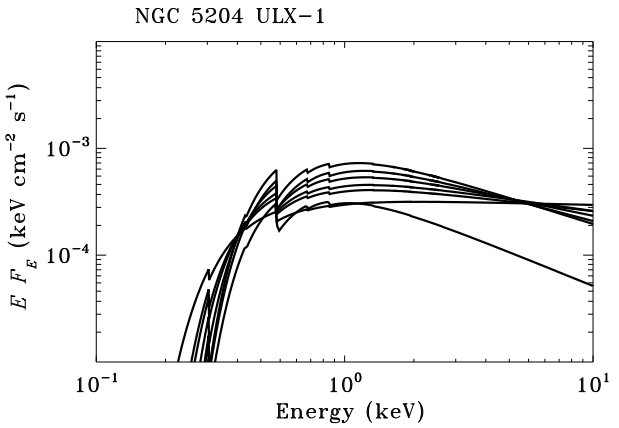


Figure 2. All observed EF_E spectra of NGC 5204 ULX-1 fitted with an absorbed POWERLAW model. The curves show the deconvolved model spectra. Spectral pivoting occurs at ~ 5.5 keV.

correlation between $L_{\rm abs}$ and Γ. Therefore, we conclude that the $L_{\rm X}-\Gamma$ correlations are real.

If the $N_{\rm H}-\Gamma$ correlation is indeed artificial, then there must be a low-energy break in the power-law component below $\sim$ 1 keV in these spectra. This could be then be interpreted as a sign that this component arises from Comptonization of the disc photons in a 'corona' surrounding the source. It is also possible, however, that the correlation between $N_{\rm H}$ and Γ has a physical origin, for example a growing luminosity might lead to a stronger outflow and therefore to a denser environment.

In general, all the sources that have luminosities *permanently above* $\sim 3\times10^{39}\,{\rm erg\,s^{-1}}$ show a power-law type spectra. In contrast, the three sources with luminosities *permanently below* $\sim 3\times10^{39}\,{\rm erg\,s^{-1}}$ have non-power-law (or thermal) type spectra (see next subsection). An exception to this 'rule' is NGC 1313 ULX-2 which has non-power-law type spectra at high luminosities and power-law type spectra at lower luminosities very much like the very high state spectra of XTE J1550-564 (Kubota & Done 2004). In some sources, both POWERLAW and DISKBB models give statistically acceptable (or equally good) fits. We assign them to a non-power-law type because their variability is consistent with Galactic black hole binaries (BHB) when modelled using DISKBB. Also, a simple absorbed POWERLAW model does not provide statistically acceptable fits for NGC 6946 X-6, but the DISKBB + POWERLAW model gives good fits for most observations (see Sect. 3.3 and Table A1). We therefore assign this source to a power-law type.

Four out of the 7 ULXs with the $L_{\rm X}-\Gamma$ correlation (NGC 1313 ULX-1, Holmberg II ULX-1, Holmberg IX ULX-1 and NGC 5204 ULX-1) show also signs of spectral pivoting. Similar pivoting has been also observed in Cyg X-1 (Zdziarski et al. 2002) and several AGNs (see e.g. Zdziarski et al. 2003, table 1, and references therein). The pivoting is clearly seen for NGC 5204 ULX-1 at ~ 5.5 keV (see Fig. 2) and the three high luminosity observations of Holmberg II ULX-1 seem to pivot at ~ 3.5 keV. The pivoting in NGC 1313 ULX-1 and Holmberg IX ULX-1 occur at the boundary of the *XMM-Newton* energy range at ~ 9 and 10 keV, respectively. To evaluate whether these pivots are real, we also show in Fig. 1 the dependences between the luminosity in a given energy band (E_1, E_2) and the photon index expected for a pivoting power-law (Zdziarski et al. 2003):

$$L_{E_1-E_2}=4\pi D^2 F_{E_1-E_2}=CE_{\rm p}^{\Gamma}\frac{E_2^{2-\Gamma}-E_1^{2-\Gamma}}{2-\Gamma}, \qquad (1)$$

where D is the distance, $F_{E_1-E_2}$ is the flux in the selected energy band and C is a constant. Equation (1) gives a good representation of the observed $L_{\rm X}-\Gamma$ relation for all these pivoting ULXs. We therefore conclude, that the pivoting is most likely real even in the cases of NGC 1313 ULX-1 and Holmberg IX ULX-1. However, when the spectrum gets very soft at $\Gamma\gtrsim 3$, NGC 1313 ULX-1, Holmberg II ULX-1 and NGC 5204 ULX-1 also show deviations from this dependence. These deviations to the low/soft states (Dewangan et al. 2004), are similar to those seen in Galactic BHBs (see Zdziarski et al. 2002, fig. 16a).

The process producing the observed power-law type spectrum is most likely Compton up-scattering of soft disc photons in a hot plasma surrounding the inner part of the disc. The observed $L_{\rm X}-\Gamma$ correlation and the pivoting in the sources can be explained by variability of the luminosity of the soft disc photons. A larger disc luminosity leads to a softer X-ray spectrum (Zdziarski et al. 2003). An example of such variability for a constant hot-plasma luminosity is given in fig. 3 of Zdziarski & Grandi (2001) for 3C 120. The similarity of this source to NGC 5204 ULX-1 (and the other 3 ULXs with pivoting) is remarkable (see Fig. 2). Transition to the low/soft state can be associated with the decreasing luminosity of the hot plasma (corona) with the nearly constant disc luminosity.

The highest quality data also seems to show a break/cutoff in the power-law component above $\sim$ 3 keV (Stobbart et al. 2006; Gladstone et al. 2009). This could be then interpreted as a sign of a cool and optically thick corona (Gladstone et al. 2009). Unfortunately the limited observing band of *XMM-Newton* and *Chandra* and the typical data quality in our sample do not allow us to see these high energy breaks/cutoffs in most of these data. A dedicated monitoring campaing of these power-law type ULXs would help us to check whether these breaks are always present, which would be highly useful in order to understand the nature of the emission mechanisms in ULXs.

3.2 Non-power-law type ULXs

Out of the selected 11 ULXs, four ULXs can be adequately fitted with an absorbed MCD model. These sources include the two ULXs that show the $L_{\rm X}-\Gamma$ anti-correlation (NGC 253 X-2 and NGC 1313 X-2) and the two low-luminosity ULXs (NGC 253 X-4 and NGC 253 X-9). The resulting fits are shown in a luminosity-temperature (hereafter $L-T$) diagram in Fig. 3 together with the observations on known BHBs adopted from Gierliński & Done (2004). These four ULXs follow the behaviour seen in BHBs. The properties of the sources can be summarised as follows.

(i) NGC 253 X-2 closely follows the $L\propto T^4$ relation. Its track on the diagram is a high luminosity–high temperature extension to XTE J1550-564 and LMC X-3. The relatively high luminosities and hot inner disc temperatures of this source compared to BHBs could be explained by assuming that this source is a maximally rotating Kerr black hole with $M\sim 70{\rm M}_\odot$ and inclination of ~ 70 degrees (Hui & Krolik 2008).

(ii) NGC 253 X-4 on the other hand behaves like LMC X-1 which clearly does not follow the expected $L\propto T^4$ relation. As discussed in Poutanen et al. (2007), this can be understood if these sources are StMBHs (or even neutron stars) accreting slightly above their Eddington accretion rates. In this case the observed temperature corresponds to the emission from the spherization radius or even the distant photosphere if observed edge-on.

(iii) NGC 253 X-9 first seems to follow the $L\propto T^4$ track at lower luminosities, but then at $L\gtrsim 10^{39}\,{\rm erg\,s^{-1}}$ deviates towards lower

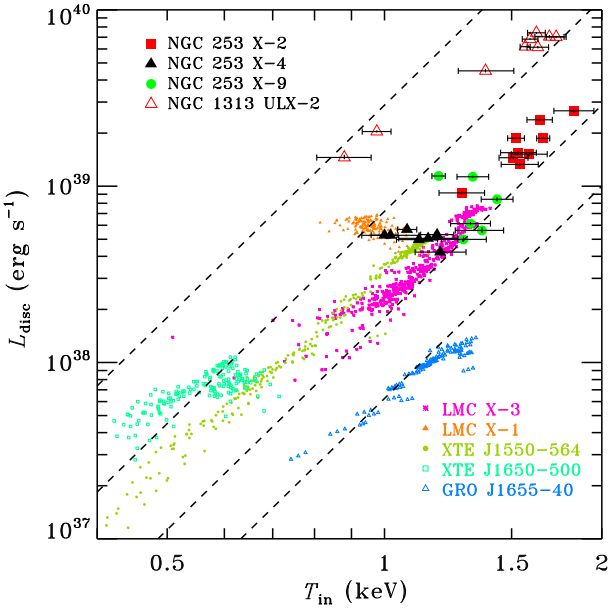


Figure 3. The MCD model luminosity-temperature diagram for the non-power-law type ULXs. All the sources roughly follow the tracks of known BHBs shown by small symbols.

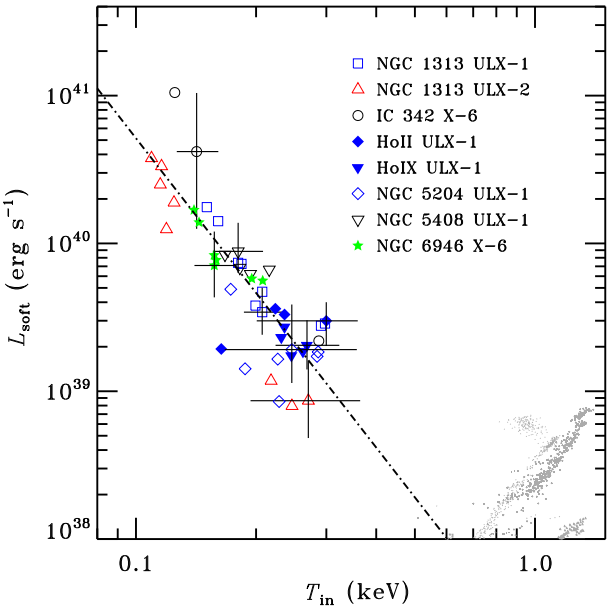


Figure 4. The luminosity-temperature diagram of the soft excess from the POWERLAW plus cool MCD model fits (only one set of errors per source is shown for clarity). All the sources with this model follow roughly a $L_{\rm soft} \propto T_{\rm in}^{-3.5}$ scaling. Note however that this scaling is subject to some modelling uncertainties (see subsection 3.3) and that the coolest and highest luminosity soft excesses of NGC 253 X-2 are artifacts of an improper modelling of the hard emission (see Fig. 5 and Table A1).

temperatures similarly to LMC X-1 and NGC 253 X-4. This type of behaviour is also seen in the spectra of XTE J1550-564 when it is in the very high state (VHS) instead of the high/soft state (Kubota & Done 2004).

(iv) NGC 1313 X-2 shows a slight deviation from the $L \propto T^4$ track much like XTE J1650-500. As the luminosity of this source greatly exceeds the Eddington limit for a 10 solar mass black hole, the simple DISKBB model is not anymore a good approximation of the spectrum. Indeed the DISKBB model failed to properly model the high-energy curvature of the spectrum, predicting slightly too steep cutoff. Because at lower luminosities the observed spectra of this source is very much like VHS spectra of XTE J1550-564 (Kubota & Done 2004), the higher luminosity non-power-law type spectra could be understood as an ultraluminous state (Roberts 2007; Soria 2007). However, a more elaborate model than the DISKBB should be used to investigate this state further.

3.3 The soft excess and the nature of ULXs

When fitting the data with the POWERLAW plus a cool MCD model, the fit improves for many (but not all) observations compared to the single component fits (see Table A1). The $L_{\rm soft} - T_{\rm in}$ relation for this soft excess is shown in Fig. 4. We find that the intrinsic luminosity of the MCD component *roughly* scales as $L_{\rm soft} \propto T_{\rm in}^{-3.5}$. The best fitting relation derived using the fitexy routine (Press et al. 1992) is $L_{\rm soft} \propto T_{\rm in}^{-3.5\pm0.2}$ with $\chi^2_{\rm red} \sim 1.09$. However, this result should be taken with some caution and there are several points to be considered.

(i) The highly luminous low-temperature excesses ($L_{\rm soft} \gtrsim 10^{40}\,{\rm erg\,s^{-1}}$, $T_{\rm in} \sim 0.1$ keV) of NGC 253 X-2 do not seem to be real features, but rather artifacts of improper modelling of the harder emission with a power-law. This results in a rise in the modelled absorption column, which then causes the increase in the estimated intrinsic luminosity of the soft excess (see Fig. 5). We therefore did not include the soft excesses of NGC 253 X-2 in deriving the best fitting $L_{\rm soft} - T_{\rm in}$ relation.

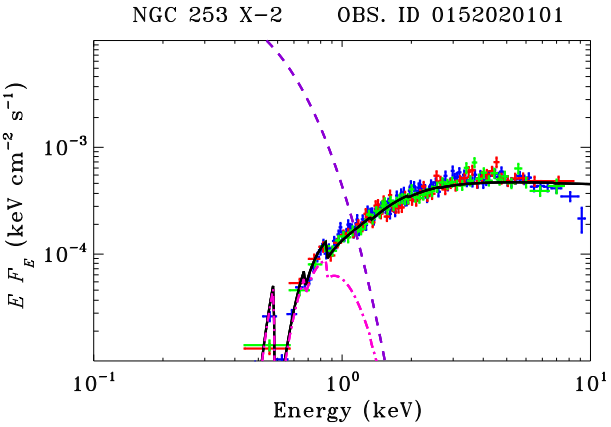


Figure 5. EF_E spectra of NGC 253 X-2 fitted with an absorbed POWERLAW plus cool MCD model. EPIC pn, mos1 and mos2 data are shown in blue, red and green, respectively. The MCD component is shown by dot-dashed line. The dashed line shows this with the effect of absorption removed. A simple absorbed MCD fit with $T_{\rm in} \sim 1.5$ keV improves the fit from $\chi^2_{\rm red} \sim 1.17$ to $\chi^2_{\rm red} \sim 1.08$. Improper modelling of the continuum by a power-law leads to almost an order of magnitude increase in the absorption column density, which produces the highly luminous cool, ~ 0.1 keV, MCD component.

(ii) As in the POWERLAW fits, $N_{\rm H}$ and Γ are still correlated for NGC 1313 ULX-1 and NGC 5204 ULX-1, but no longer for Holmberg IX ULX-1. As discussed earlier (see subsection 3.1), there is no clear evidence whether this correlation has a physical origin, or the power-law component has a low-energy break, what one would expect at about $T_{\rm in}$, if it arises from Comptonization of the

disc photons in a corona. If such break would exist in the power-law component (note that $\Gamma \gtrsim 2$ for NGC 1313 ULX-1 and NGC 5204 ULX-1), then it would necessarily lead to both lower absorption columns and higher *absorbed* MCD component luminosities to compensate the 'loss' of flux at low energies. But on the other hand, the decrease in $N_{\rm H}$ could then ultimately lead to lower *deabsorbed* luminosities $L_{\rm soft}$.
(iii) If one interprets the spectra in terms of an outflow model (Poutanen et al. 2007), one would then expect an increase of $N_{\rm H}$ with the luminosity because the outflow would increase the column depth. Also, $N_{\rm H}$ could be then inversely proportional to $T_{\rm in}$, as it should decrease with increasing luminosity.
(iv) The host galaxy distances have some uncertainties, which can lead to systematic errors in the derived luminosities.
(v) The MCD component appears at low energies, where the calibration of *XMM-Newton* and *Chandra* are the least accurate. Also, at these energies the correct estimation of the absorption column makes the most difference in the derived parameter values of the MCD component.
(vi) In addition to these complications, the selection of the lower energy bound in the spectral fitting also has some effect. For example, there are some discrepancies between our results of NGC 5204 ULX-1 and those of Feng & Kaaret (2009), who used 0.2 keV as a lower energy bound in their fitting.

All these factors cast a doubt on the derived best fitting relation $L_{\rm soft} \propto T_{\rm in}^{-3.5\pm0.2}$, but the overall trend of cooler discs with higher luminosities at $L_{\rm soft} \lesssim 10^{40}\,{\rm erg\,s^{-1}}$ and $T_{\rm in} \gtrsim 0.1$ keV seems to be real. However, the observed trend (whether or not it has a power-law index -3.5 or something close) is not consistent with the interpretation of an accretion disc around an IMBH. If the observed soft excess does not originate from a disc around an IMBH, what is its origin? One possible explanation could be that the thermal emission arises from the spherization radius of a super-Eddington disc with an outflow (Poutanen et al. 2007). As observed, this model predicts that the thermal emission becomes cooler with increasing luminosity. Although the observed trend is too steep for the predicted relation of this model (Poutanen et al. 2007, eqs. 19, 36–38), the apparent luminosity of this component might be overestimated because the outflowing wind causes some of the emission to be beamed. Indeed, King & Puchnarewicz (2002) showed that at low inclination angles an outflow causes the observed luminosity to be

$$L_{\rm obs} = 2.3\times10^{44}\left(\frac{T}{0.1{\rm keV}}\right)^{-4}\frac{l^2}{pbr^2}\,{\rm erg\,s^{-1}}, \quad (2)$$

where the luminosity is scaled to the Eddington value $l = L/L_{\rm Edd}$, p is a factor allowing for deviation from the spherical symmetry, r is the radius scaled to the Schwarzschild radius $r = R/R_{\rm s}$ ($R_{\rm s} = 2GM/c^2$) and b is the beaming factor. Assuming that $L_{\rm soft} = L_{\rm obs}$, King (2009) argued that the beaming factor has to scale as $b \propto \dot{m}^{-2}$, where the accretion rate is scaled to its Eddington value $\dot{m} = \dot{M}/\dot{M}_{\rm Edd}$, to satisfy the observed relation $L_{\rm soft} \sim 7\times10^{40}T_{\rm in}^{-4}$ based on the results of Kajava & Poutanen (2008). Using this scaling, King (2009) estimated the mass of the accreting black hole

$$\frac{M}{{\rm M}_\odot} = x\frac{4500}{\dot{m}^2(1+\ln\dot{m})}\frac{L_{\rm soft}}{10^{40}\,{\rm erg\,s^{-1}}}, \quad (3)$$

where the factor x is the order of unity (see King 2009, eq. 7). In our view, however, the estimation of the black hole mass given by equation (3) must be taken with caution, because of the possible systematic uncertainties in the derived best fitting parameters of the MCD component. Never the less, we conclude that our observational data is consistent with the idea that the most luminous sources in our sample are $\sim 10{\rm M}_\odot$ black holes accreting at mildly super-Eddington rates $\dot{m} \sim 10$ and viewed at low inclinations.

The ULXs that have this soft excess in our sample have a power-law type spectra. This spectrum most likely arises from Comptonization of the disc photons in a corona surrounding the central parts (within the spherization radius) of the accretion flow (Haardt & Maraschi 1993; Poutanen & Svensson 1996). Another possibility for the power-law spectra could be due to overheating of the accreting gas close to accreting black hole (Beloborodov 1998). Therefore, a plausible explanation to both the observed $L_{\rm soft} - T_{\rm in}$ relation and power-law type spectra could be that at low inclinations the central Comptonized part of the disc would be visible to the observer at all times and the outflowing wind would cause the Comptonized emission and the emission from the spherization radius to be geometrically beamed, thus resulting in a high $\sim 10^{40}\,{\rm erg\,s^{-1}}$ apparent luminosity. On the other hand, at higher inclinations the central part of the disc would be obscured by the outflow. This would result in a non-power-law type spectra that we see for NGC 253 X-4 and NGC 253 X-9.

4 CONCLUSIONS

We have studied spectral variability of 11 ULXs and can draw several conclusions.

(i) The ULXs of this sample can be roughly separated into two types based on their spectra: power-law- and non-power-law type ULXs. All the power-law type ULXs are constantly more luminous than $\sim 3\times10^{39}\,{\rm erg\,s^{-1}}$, i.e. they show permanently super-Eddington luminosities for a $\sim 10{\rm M}_\odot$ black hole.
(ii) Six out of the seven power-law type ULXs show a $L_{\rm X} - \Gamma$ correlation, i.e. the observed spectrum softens as the luminosity increases. Furthermore, four ULXs show also spectral pivoting with pivot energies $E_{\rm p} \lesssim 10$ keV. Three ULXs (NGC 1313 ULX-1, Holmberg II ULX-1 and NGC 5204 ULX-1) also show state transitions to a low/soft state.
(iii) The non-power-law type ULXs can be adequately modelled with a MCD. These sources also follow the behaviour of known BHBs in the $L - T$ diagrams.
(iv) NGC 1313 ULX-2 is a very interesting source showing a VHS type spectra (similar to XTE J1550-564) at lower luminosities and a non-power-law (thermal) like spectra at high luminosities. It is the only source in this sample showing transitions between a spectral state that is seen in known BHBs and an ultraluminous spectral state. NGC 1313 ULX-2 is therefore most likely a super-Eddington source.
(v) The soft excess seems to roughly follow a trend $L_{\rm soft} \propto T_{\rm in}^{-3.5}$, which does not support the idea that the observed soft excess arises from the disc emission around IMBHs. Instead, the soft excess in consistent with beamed disc emission from the spherization radius.

We therefore conclude that the ULXs are most likely powered by super-Eddington accretion onto $\sim 10{\rm M}_\odot$ black holes. The two different types of ULXs result from their different inclination angles. The permanently super-Eddington power-law type ULXs might be viewed at low inclination angles. The low-luminosity ULXs with non-power-law spectra are consistent of being super-Eddington sources viewed at high inclinations (NGC 253 X-4,

NGC 253 X-9) or they are sub-Eddington sources (NGC 253 X-2).

ACKNOWLEDGEMENTS

The authors thank Dr. Hua Feng and the anonymous referee for useful comments. This work was supported by the Finnish Graduate School in Astronomy and Space Physics (JJEK) and the Academy of Finland grant 127512 (JP). This research has made use of data obtained from the Chandra Data Archive and software provided by the Chandra X-ray Center (CXC) in the application packages CIAO, ChIPS, and Sherpa. This research was based on observations obtained with XMM-Newton, an ESA science mission with instruments and contributions directly funded by ESA Member States and NASA.

REFERENCES

Abolmasov P., Fabrika S., Sholukhova O., Afanasiev V., 2007, Astrophysical Bulletin, 62, 36
Abramowicz M. A., Czerny B., Lasota J. P., Szuszkiewicz E., 1988, ApJ, 332, 646
Arons J., 1992, ApJ, 388, 561
Begelman M. C., 2001, ApJ, 551, 897
Belczynski K., Bulik T., Fryer C. L., Ruiter A., Vink J. S., Hurley J. R., 2009, arXiv:0904.2784
Beloborodov A. M., 1998, MNRAS, 297, 739
Berghea C. T., Weaver K. A., Colbert E. J. M., Roberts T. P., 2008, ApJ, 687, 471
Dewangan G. C., Griffiths R. E., Rao A. R., 2006, ApJ, 641, L125
Dewangan G. C., Miyaji T., Griffiths R. E., Lehmann I., 2004, ApJ, 608, L57
Dickey J. M., Lockman F. J., 1990, ARA&A, 28, 215
Fabbiano G., 1989, ARA&A, 27, 87
Fabbiano G., Zezas A., King A. R., Ponman T. J., Rots A., Schweizer F., 2003, ApJ, 584, L5
Feng H., Kaaret P., 2005, ApJ, 633, 1052
Feng H., Kaaret P., 2006a, ApJ, 653, 536
Feng H., Kaaret P., 2006b, ApJ, 650, L75
Feng H., Kaaret P., 2007, ApJ, 660, L113
Feng H., Kaaret P., 2009, ApJ, 696, 1712
Freeland M., Kuncic Z., Soria R., Bicknell G. V., 2006, MNRAS, 372, 630
Gierliński M., Done C., 2004, MNRAS, 347, 885
Gladstone J. C., Roberts T. P., Done C., 2009, MNRAS, in press (arXiv:0905.4076)
Goad M. R., Roberts T. P., Reeves J. N., Uttley P., 2006, MNRAS, 365, 191
Gonçalves A. C., Soria R., 2006, MNRAS, 371, 673
Haardt F., Maraschi L., 1993, ApJ, 413, 507
Hui Y., Krolik J. H., 2008, ApJ, 679, 1405
Jaroszyński M., Abramowicz M. A., Paczyński B., 1980, Acta Astronomica, 30, 1
Kaaret P., Corbel S., 2009, arXiv:0903.5329
Kaaret P., Corbel S., Prestwich A. H., Zezas A., 2003, Science, 299, 365
Kaaret P., Ward M. J., Zezas A., 2004, MNRAS, 351, L83
Kajava J. J. E., Poutanen J., 2008, in Axelsson M., ed, AIP Conf. Series Vol. 1054, Cool Discs, Hot Flows: The Varying Faces of Accreting Compact Objects. Am. Inst. Phys., New York, p. 39
Karachentsev I. D., Dolphin A. E., Geisler D. et al., 2002, A&A, 383, 125
Kawaguchi T., 2003, ApJ, 593, 69
King A. R., 2009, MNRAS, 393, L41
King A. R., Davies M. B., Ward M. J., Fabbiano G., Elvis M., 2001, ApJ, 552, L109
King A. R., Puchnarewicz E. M., 2002, MNRAS, 336, 445
Körding E., Falcke H., Markoff S., 2002, A&A, 382, L13
Kubota A., Done C., 2004, MNRAS, 353, 980
Liu J., 2008, arXiv:0811.0804
Liu J.-F., Bregman J. N., 2005, ApJS, 157, 59
Liu Q. Z., Mirabel I. F., 2005, A&A, 429, 1125
Miller J. M., Fabbiano G., Miller M. C., Fabian A. C., 2003, ApJ, 585, L37
Miller M. C., Colbert E. J. M., 2004, International Journal of Modern Physics D, 13, 1
Mushotzky R., 2006, Advances in Space Research, 38, 2793
Pakull M. W., Mirioni L., 2003, Rev. Mex. AA Conf. Ser., 15, 197
Patruno A., Portegies Zwart S., Dewi J., Hopman C., 2006, MNRAS, 370, L6
Poutanen J., Lipunova G., Fabrika S., Butkevich A. G., Abolmasov P., 2007, MNRAS, 377, 1187
Poutanen J., Svensson R., 1996, ApJ, 470, 249
Press W. H., Teukolsky S. A., Vetterling W. T., Flannery B. P., 1992, Numerical recipes in FORTRAN. The art of scientific computing. Cambridge: University Press, 2nd ed.
Roberts T. P., 2007, Ap&SS, 311, 203
Roberts T. P., Kilgard R. E., Warwick R. S., Goad M. R., Ward M. J., 2006, MNRAS, 371, 1877
Roberts T. P., Levan A. J., Goad M. R., 2008, MNRAS, 387, 73
Shakura N. I., Sunyaev R. A., 1973, A&A, 24, 337
Soria R., 2007, Ap&SS, 311, 213
Stobbart A.-M., Roberts T. P., Wilms J., 2006, MNRAS, 368, 397
Strohmayer T. E., Mushotzky R. F., 2003, ApJ, 586, L61
Strohmayer T. E., Mushotzky R. F., Winter L., Soria R., Uttley P., Cropper M., 2007, ApJ, 660, 580
Vierdayanti K., Mineshige S., Ebisawa K., Kawaguchi T., 2006, PASJ, 58, 915
Vikhlinin A., Churazov E., Gilfanov M. et al., 1994, ApJ, 424, 395
Winter L. M., Mushotzky R. F., Reynolds C. S., 2006, ApJ, 649, 730
Zdziarski A. A., Grandi P., 2001, ApJ, 551, 186
Zdziarski A. A., Lubiński P., Gilfanov M., Revnivtsev M., 2003, MNRAS, 342, 355
Zdziarski A. A., Poutanen J., Paciesas W. S., Wen L., 2002, ApJ, 578, 357

APPENDIX A: BEST-FITTING MODEL PARAMETERS

Table A1: Best-fitting parameters and absorption corrected luminosity estimates. The results are given only if $\chi^2_{\rm red} < 2$. In the case of the POWERLAW + DISKBB model, the results are given if the soft excess DISKBB component is constrained.

Obs.ID	$N_{\rm H}$ [b]	Γ [c]	$T_{\rm in}$ [d]	$L_{\rm power-law}$ [e]	$L_{\rm diskbb}$ [f]	$\chi^2_{\rm red}$ | d.o.f. [g]	$P_{\rm rej}$ [h]
			NGC 253 X-2				
790	$1.4^{+0.3}_{-0.3}$	...	$1.28^{+0.10}_{-0.09}$	...	$0.92^{+0.02}_{-0.02}$	1.80 | 105	100.0%
	$4.0^{+0.5}_{-0.5}$	$2.1^{+0.1}_{-0.1}$	...	$1.37^{+0.07}_{-0.06}$	...	1.26 | 105	96.2%
	$5.7^{+2.0}_{-1.5}$	$2.0^{+0.2}_{-0.2}$	$0.22^{+0.10}_{-0.06}$	$1.3^{+0.2}_{-0.2}$	$1.1^{+3.8}_{-0.8}$	1.19 | 103	90.3%
0110900101	$1.7^{+0.2}_{-0.2}$	...	$1.64^{+0.07}_{-0.06}$	...	$2.38^{+0.04}_{-0.04}$	1.09 | 348	88.1%
	$3.7^{+0.3}_{-0.3}$	$1.76^{+0.05}_{-0.05}$	...	$3.0^{+0.1}_{-0.1}$	...	1.18 | 348	98.7%
	$8.7^{+1.2}_{-1.2}$	$2.1^{+0.1}_{-0.1}$	$0.10^{+0.01}_{-0.01}$	$3.8^{+0.3}_{-0.3}$	92^{+142}_{-56}	1.05 | 346	76.3%
0125960101	$1.56^{+0.11}_{-0.11}$	...	$1.52^{+0.04}_{-0.04}$	...	$1.87^{+0.02}_{-0.02}$	0.95 | 583	18.2%
	$3.7^{+0.2}_{-0.2}$	$1.89^{+0.04}_{-0.04}$	...	$2.37^{+0.05}_{-0.05}$	...	1.24 | 583	100.0%
	$9.3^{+0.8}_{-0.8}$	$2.26^{+0.06}_{-0.06}$	$0.09^{+0.01}_{-0.01}$	$3.4^{+0.3}_{-0.2}$	202^{+195}_{-89}	1.01 | 581	58.9%
0125960201	$1.8^{+0.3}_{-0.3}$	...	$1.83^{+0.12}_{-0.11}$	...	$2.68^{+0.07}_{-0.07}$	0.97 | 160	41.5%
	$3.7^{+0.5}_{-0.5}$	$1.66^{+0.08}_{-0.08}$	...	$3.15^{+0.14}_{-0.13}$	...	1.25 | 160	98.1%
	$8.9^{+1.7}_{-1.7}$	$2.0^{+0.1}_{-0.1}$	$0.09^{+0.01}_{-0.01}$	$4.0^{+0.5}_{-0.4}$	189^{+519}_{-138}	1.04 | 158	63.9%
0152020101	$1.65^{+0.08}_{-0.08}$	...	$1.66^{+0.03}_{-0.03}$	...	$1.87^{+0.02}_{-0.01}$	1.08 | 934	95.8%
	$3.7^{+0.14}_{-0.14}$	$1.80^{+0.03}_{-0.03}$	...	$2.28^{+0.03}_{-0.03}$	...	1.32 | 934	100.0%
	$8.2^{+0.6}_{-0.6}$	$2.08^{+0.05}_{-0.05}$	$0.10^{+0.01}_{-0.01}$	$2.9^{+0.1}_{-0.1}$	55^{+36}_{-21}	1.17 | 932	100.0%
0304850901	$2.0^{+0.3}_{-0.3}$	...	$1.53^{+0.09}_{-0.08}$	...	$1.55^{+0.03}_{-0.02}$	1.02 | 166	59.1%
	$4.3^{+0.5}_{-0.5}$	$1.89^{+0.09}_{-0.08}$	...	$2.05^{+0.11}_{-0.09}$	...	1.22 | 166	97.0%
	$9.2^{+2.0}_{-1.9}$	$2.21^{+0.15}_{-0.14}$	$0.09^{+0.01}_{-0.01}$	$2.8^{+0.5}_{-0.4}$	100^{+316}_{-76}	1.10 | 164	80.8%
0304851001	$1.5^{+0.2}_{-0.2}$	...	$1.59^{+0.09}_{-0.09}$	...	$1.52^{+0.03}_{-0.03}$	0.79 | 168	1.9%
	$3.5^{+0.4}_{-0.4}$	$1.82^{+0.08}_{-0.08}$	...	$1.91^{+0.08}_{-0.07}$	...	0.89 | 168	16.8%
	$8.0^{+1.7}_{-1.7}$	$2.09^{+0.13}_{-0.13}$	$0.10^{+0.02}_{-0.01}$	$2.4^{+0.3}_{-0.3}$	46^{+132}_{-35}	0.80 | 166	2.9%
0304851101	$1.3^{+0.3}_{-0.2}$	...	$1.54^{+0.09}_{-0.09}$	...	$1.33^{+0.03}_{-0.03}$	0.96 | 168	36.4%
	$3.2^{+0.4}_{-0.4}$	$1.79^{+0.08}_{-0.08}$	...	$1.67^{+0.09}_{-0.08}$	...	1.21 | 168	96.9%
	$9.1^{+1.6}_{-1.6}$	$2.20^{+0.14}_{-0.14}$	$0.09^{+0.01}_{-0.01}$	$2.4^{+0.4}_{-0.3}$	142^{+379}_{-104}	1.03 | 166	62.6%
0304851201	$1.5^{+0.2}_{-0.2}$	...	$1.51^{+0.07}_{-0.07}$	...	$1.45^{+0.02}_{-0.02}$	1.12 | 247	89.8%
	$3.5^{+0.3}_{-0.3}$	$1.84^{+0.07}_{-0.07}$	...	$1.85^{+0.07}_{-0.06}$	...	1.39 | 247	100.0%
	$8.1^{+1.2}_{-1.2}$	$2.18^{+0.11}_{-0.11}$	$0.09^{+0.01}_{-0.01}$	$2.5^{+0.3}_{-0.2}$	99^{+191}_{-64}	1.23 | 245	99.1%
			NGC 253 X-4				
790	$2.3^{+0.5}_{-0.5}$	...	$1.12^{+0.08}_{-0.08}$	...	$0.50^{+0.02}_{-0.02}$	0.85 | 62	21.4%
	$5.5^{+0.8}_{-0.7}$	$2.37^{+0.14}_{-0.14}$	...	$0.83^{+0.10}_{-0.08}$	...	1.08 | 62	69.5%
0110900101	$2.0^{+0.5}_{-0.5}$	...	$1.19^{+0.10}_{-0.09}$	...	$0.42^{+0.01}_{-0.01}$	0.70 | 88	1.5%
	$5.0^{+0.8}_{-0.8}$	$2.21^{+0.15}_{-0.14}$	...	$0.69^{+0.08}_{-0.07}$	...	0.80 | 88	8.6%
0125960101	$3.2^{+0.3}_{-0.3}$	...	$1.00^{+0.04}_{-0.04}$	...	$0.53^{+0.01}_{-0.01}$	1.07 | 260	78.7%
	$7.1^{+0.6}_{-0.5}$	$2.67^{+0.09}_{-0.09}$	...	$1.1^{+0.1}_{-0.1}$	...	1.18 | 260	97.4%
0152020101	$3.2^{+0.2}_{-0.2}$	...	$1.07^{+0.03}_{-0.03}$	...	$0.57^{+0.01}_{-0.01}$	0.95 | 497	22.8%
	$7.0^{+0.4}_{-0.4}$	$2.54^{+0.07}_{-0.06}$	...	$1.08^{+0.07}_{-0.06}$	...	1.20 | 497	99.8%
3931	$2.2^{+0.3}_{-0.3}$	...	$1.18^{+0.06}_{-0.06}$	...	$0.53^{+0.01}_{-0.01}$	1.05 | 133	67.0%
	$4.9^{+0.5}_{-0.4}$	$2.2^{+0.1}_{-0.1}$	...	$0.81^{+0.05}_{-0.04}$	...	1.26 | 133	97.8%
0304850901	$2.2^{+0.6}_{-0.5}$	...	$1.15^{+0.11}_{-0.10}$	...	$0.51^{+0.02}_{-0.02}$	0.73 | 75	4.0%
	$5.3^{+1.0}_{-0.9}$	$2.3^{+0.2}_{-0.2}$	...	$0.83^{+0.12}_{-0.09}$	...	0.83 | 75	14.4%
0304851001	$3.4^{+0.8}_{-0.7}$	...	$1.02^{+0.10}_{-0.09}$	...	$0.53^{+0.03}_{-0.02}$	1.15 | 76	81.9%
	$7.2^{+1.3}_{-1.1}$	$2.5^{+0.2}_{-0.2}$	...	$1.0^{+0.2}_{-0.2}$	...	1.14 | 76	80.4%
			NGC 253 X-9				
0110900101	$1.6^{+0.4}_{-0.3}$	$2.4^{+0.2}_{-0.2}$	...	$0.41^{+0.04}_{-0.04}$	...	1.25 | 104	95.5%
0125960101	$0.37^{+0.18}_{-0.17}$	...	$1.33^{+0.07}_{-0.07}$	...	$1.13^{+0.02}_{-0.02}$	0.99 | 173	46.1%
	$2.2^{+0.3}_{-0.3}$	$1.93^{+0.08}_{-0.07}$	...	$1.53^{+0.06}_{-0.05}$	...	1.24 | 173	98.3%
0152020101	$0.41^{+0.06}_{-0.06}$	...	$1.19^{+0.03}_{-0.03}$	...	$1.14^{+0.01}_{-0.01}$	1.14 | 821	99.7%
	$2.4^{+0.1}_{-0.1}$	$2.12^{+0.03}_{-0.03}$	...	$1.63^{+0.03}_{-0.03}$	...	1.20 | 821	100.0%

Continued on next page...

Table A1 – Continued

Obs.ID	$N_{\rm H}$ [a]	Γ [b]	$T_{\rm in}$ [c]	$L_{\rm power-law}$ [d]	$L_{\rm diskbb}$ [e]	$\chi^2_{\rm red}$ | d.o.f. [f]	$P_{\rm rej}$ [g]
3931	$0.3^{+0.1}_{-0.1}$	...	$1.43^{+0.07}_{-0.07}$	...	$0.84^{+0.02}_{-0.02}$	1.31 | 180	99.7%
	$1.8^{+0.2}_{-0.2}$	$1.74^{+0.06}_{-0.06}$	...	$1.11^{+0.01}_{-0.01}$	...	1.07 | 180	74.2%
0304850901	$0.17^{+0.25}_{-0.03}$	...	$1.29^{+0.10}_{-0.10}$	...	$0.50^{+0.02}_{-0.01}$	1.03 | 90	58.9%
	$1.8^{+0.4}_{-0.4}$	$1.93^{+0.1}_{-0.1}$	...	$0.66^{+0.04}_{-0.03}$	...	1.25 | 90	94.6%
0304851001	$0.14^{+0.22}_{-0.01}$	...	$1.36^{+0.10}_{-0.11}$	...	$0.56^{+0.02}_{-0.02}$	1.06 | 100	69.0%
	$1.8^{+0.4}_{-0.3}$	$1.88^{+0.1}_{-0.1}$	...	$0.75^{+0.03}_{-0.03}$	...	1.00 | 100	50.7%
0304851201	$0.4^{+0.2}_{-0.2}$	...	$1.32^{+0.09}_{-0.08}$	...	$0.61^{+0.01}_{-0.01}$	1.02 | 156	57.4%
	$2.2^{+0.3}_{-0.3}$	$1.93^{+0.1}_{-0.1}$	...	$0.83^{+0.04}_{-0.04}$	...	1.14 | 156	89.3%
			NGC 1313 ULX-1				
0106860101	$1.70^{+0.09}_{-0.09}$	$1.86^{+0.03}_{-0.03}$	...	$5.52^{+0.07}_{-0.06}$	...	1.16 | 810	99.9%
	$2.7^{+0.4}_{-0.3}$	$1.71^{+0.05}_{-0.05}$	$0.21^{+0.03}_{-0.02}$	$5.3^{+0.2}_{-0.2}$	$3.4^{+1.6}_{-1.0}$	0.99 | 808	42.9%
0150280301	$3.4^{+0.2}_{-0.2}$	$2.42^{+0.07}_{-0.07}$	...	$15.2^{+0.6}_{-0.6}$	...	0.99 | 261	44.8%
	$4.0^{+0.9}_{-0.6}$	$2.36^{+0.10}_{-0.10}$	$0.18^{+0.08}_{-0.04}$	$14.7^{+1.4}_{-1.3}$	7^{+19}_{-5}	0.96 | 259	34.8%
0150280401	$3.7^{+0.4}_{-0.4}$	$2.4^{+0.1}_{-0.1}$	...	$12.5^{+1.0}_{-0.8}$	...	0.95 | 88	39.8%
	$4.4^{+1.9}_{-1.0}$	$2.3^{+0.2}_{-0.2}$	$0.18^{+0.18}_{-0.06}$	$12.1^{+2.4}_{-2.0}$	7^{+19}_{-5}	0.94 | 86	37.0%
0150280601	$3.0^{+0.2}_{-0.2}$	$2.31^{+0.08}_{-0.08}$	...	$10.8^{+0.5}_{-0.4}$	...	0.99 | 195	49.1%
	$3.0^{+0.6}_{-0.6}$	$2.1^{+0.2}_{-0.3}$	$0.29^{+0.12}_{-0.09}$	$9.0^{+1.4}_{-1.8}$	$2.8^{+2.7}_{-1.5}$	0.96 | 193	34.4%
0150281101	$3.2^{+0.2}_{-0.2}$	$2.35^{+0.07}_{-0.07}$	...	$12.0^{+0.6}_{-0.6}$	...	0.92 | 262	19.7%
0205230201	$2.3^{+0.4}_{-0.3}$	$2.06^{+0.12}_{-0.11}$	...	$6.1^{+0.3}_{-0.3}$	...	1.16 | 104	87.8%
	$4.7^{+1.8}_{-1.7}$	$2.0^{+0.2}_{-0.2}$	$0.15^{+0.08}_{-0.03}$	$6.3^{+1.1}_{-0.9}$	18^{+86}_{-15}	1.04 | 102	63.7%
0205230301	$3.4^{+0.2}_{-0.2}$	$2.31^{+0.06}_{-0.05}$	...	$17.8^{+0.7}_{-0.6}$	...	0.98 | 302	41.3%
0205230401	$3.9^{+0.3}_{-0.2}$	$3.3^{+0.1}_{-0.1}$	...	$9.4^{+1.1}_{-0.9}$	...	1.18 | 238	97.0%
	$4.6^{+0.8}_{-0.6}$	$3.0^{+0.2}_{-0.2}$	$0.16^{+0.03}_{-0.02}$	$6.9^{+1.4}_{-1.3}$	14^{+20}_{-7}	1.03 | 236	63.7%
0205230501	$2.2^{+0.2}_{-0.2}$	$2.04^{+0.08}_{-0.07}$	...	$7.5^{+0.2}_{-0.2}$	...	1.10 | 212	85.9%
	$2.4^{+0.6}_{-0.5}$	$1.7^{+0.2}_{-0.2}$	$0.30^{+0.08}_{-0.07}$	$6.3^{+0.6}_{-0.6}$	$2.9^{+1.6}_{-0.9}$	0.97 | 210	39.8%
0205230601	$1.9^{+0.2}_{-0.2}$	$1.92^{+0.06}_{-0.06}$	...	$6.2^{+0.1}_{-0.1}$	...	1.18 | 331	98.6%
	$3.0^{+0.7}_{-0.6}$	$1.74^{+0.10}_{-0.10}$	$0.21^{+0.04}_{-0.03}$	$5.9^{+0.3}_{-0.3}$	$4.7^{+4.3}_{-2.0}$	1.03 | 329	63.9%
0405090101	$1.79^{+0.04}_{-0.04}$	$1.86^{+0.02}_{-0.02}$	...	$5.37^{+0.03}_{-0.03}$	...	1.34 | 1514	100.0%
	$2.9^{+0.2}_{-0.2}$	$1.73^{+0.03}_{-0.03}$	$0.20^{+0.01}_{-0.01}$	$5.2^{+0.1}_{-0.1}$	$3.8^{+0.8}_{-0.7}$	1.01 | 1512	58.8%
			NGC 1313 ULX-2				
0106860101	$2.5^{+0.2}_{-0.2}$	$2.4^{+0.1}_{-0.1}$	...	$2.5^{+0.1}_{-0.1}$	...	0.98 | 172	44.1%
	$2.5^{+0.6}_{-0.5}$	$2.1^{+0.2}_{-0.3}$	$0.27^{+0.09}_{-0.08}$	$2.0^{+0.3}_{-0.4}$	$0.9^{+0.7}_{-0.4}$	0.91 | 170	21.5%
0150280101	$0.9^{+0.3}_{-0.3}$	...	$1.4^{+0.1}_{-0.1}$	...	$4.5^{+0.1}_{-0.1}$	1.03 | 78	60.4%
	$2.6^{+0.5}_{-0.5}$	$1.8^{+0.1}_{-0.1}$	...	$6.2^{+0.4}_{-0.4}$	...	1.10 | 78	74.0%
0150280301	$0.86^{+0.10}_{-0.10}$	...	$1.63^{+0.06}_{-0.05}$	...	$6.1^{+0.1}_{-0.1}$	1.18 | 450	99.4%
	$2.6^{+0.2}_{-0.2}$	$1.76^{+0.04}_{-0.04}$	...	$7.5^{+0.1}_{-0.1}$	...	1.07 | 450	84.8%
	$4.4^{+0.9}_{-1.0}$	$1.89^{+0.07}_{-0.08}$	$0.12^{+0.02}_{-0.01}$	$8.2^{+0.5}_{-0.4}$	12^{+21}_{-9}	1.05 | 448	78.9%
0150280401	$0.86^{+0.14}_{-0.13}$	...	$1.69^{+0.08}_{-0.08}$	...	$7.0^{+0.2}_{-0.2}$	1.04 | 284	69.4%
	$2.5^{+0.2}_{-0.2}$	$1.71^{+0.06}_{-0.05}$	...	$8.5^{+0.2}_{-0.2}$	...	0.95 | 284	27.4%
0150280501	$2.3^{+0.3}_{-0.3}$	$2.1^{+0.1}_{-0.1}$	...	$3.9^{+0.3}_{-0.3}$	...	1.14 | 133	87.0%
0150280601	$0.52^{+0.14}_{-0.11}$	...	$0.98^{+0.05}_{-0.04}$	...	$2.04^{+0.03}_{-0.03}$	1.15 | 232	93.9%
	$2.8^{+0.2}_{-0.2}$	$2.4^{+0.1}_{-0.1}$	...	$3.3^{+0.2}_{-0.2}$	...	0.85 | 232	4.6%
0150281101	$2.4^{+0.4}_{-0.3}$	$2.3^{+0.1}_{-0.1}$	...	$2.7^{+0.2}_{-0.2}$	...	0.97 | 116	43.6%
0205230201	$0.6^{+0.4}_{-0.2}$	...	$0.88^{+0.08}_{-0.07}$	...	$1.46^{+0.05}_{-0.03}$	1.27 | 58	91.7%
	$3.2^{+0.6}_{-0.5}$	$2.6^{+0.2}_{-0.2}$	...	$2.7^{+0.4}_{-0.3}$	...	1.17 | 58	82.3%
0205230301	$1.1^{+0.1}_{-0.1}$	...	$1.62^{+0.05}_{-0.05}$	...	$7.4^{+0.1}_{-0.1}$	1.11 | 580	96.1%
	$3.0^{+0.2}_{-0.1}$	$1.81^{+0.04}_{-0.04}$	...	$9.2^{+0.2}_{-0.2}$	...	1.05 | 580	82.4%
	$4.9^{+0.8}_{-0.9}$	$1.92^{+0.06}_{-0.06}$	$0.12^{+0.01}_{-0.01}$	$10.0^{+0.5}_{-0.5}$	18^{+24}_{-12}	1.04 | 578	74.8%
0205230401	$1.7^{+0.3}_{-0.3}$	$2.2^{+0.1}_{-0.1}$	...	$1.9^{+0.1}_{-0.1}$	...	0.93 | 135	29.6%
	$2.0^{+1.1}_{-0.8}$	$1.9^{+0.2}_{-0.3}$	$0.25^{+0.13}_{-0.08}$	$1.6^{+0.3}_{-0.3}$	$0.8^{+1.8}_{-0.4}$	0.87 | 133	13.5%
0205230501	$2.5^{+0.2}_{-0.2}$	$2.36^{+0.07}_{-0.07}$	...	$2.45^{+0.1}_{-0.1}$	...	1.05 | 270	70.9%
	$2.8^{+0.7}_{-0.5}$	$2.2^{+0.1}_{-0.2}$	$0.22^{+0.08}_{-0.05}$	$2.1^{+0.2}_{-0.3}$	$1.2^{+1.9}_{-0.6}$	0.98 | 268	43.0%
0205230601	$1.05^{+0.1}_{-0.1}$	...	$1.73^{+0.06}_{-0.05}$	...	$7.0^{+0.1}_{-0.1}$	1.08 | 536	90.4%
	$2.8^{+0.2}_{-0.2}$	$1.71^{+0.04}_{-0.04}$	...	$8.4^{+0.1}_{-0.1}$	...	1.07 | 536	88.0%

Continued on next page...

Table A1 – Continued

Obs.ID	$N_{\rm H}$ [a]	Γ [b]	$T_{\rm in}$ [c]	$L_{\rm power-law}$ [d]	$L_{\rm diskbb}$ [e]	$\chi^2_{\rm red}$ | d.o.f. [f]	$P_{\rm rej}$ [g]
	$5.4^{+0.8}_{-0.9}$	$1.87^{+0.06}_{-0.07}$	$0.12^{+0.01}_{-0.01}$	$9.4^{+0.5}_{-0.4}$	33^{+37}_{-19}	1.03 | 534	71.7%
0301860101	$1.2^{+0.1}_{-0.1}$	...	$1.59^{+0.04}_{-0.04}$	...	$6.82^{+0.07}_{-0.07}$	1.07 | 712	90.5%
	$3.12^{+0.14}_{-0.13}$	$1.83^{+0.03}_{-0.03}$	...	$8.5^{+0.1}_{-0.1}$	...	1.15 | 712	99.7%
	$5.6^{+0.6}_{-0.7}$	$2.00^{+0.05}_{-0.05}$	$0.11^{+0.01}_{-0.01}$	$9.7^{+0.4}_{-0.4}$	38^{+32}_{-19}	1.10 | 710	96.1%
0405090101	$1.03^{+0.05}_{-0.04}$	...	$1.57^{+0.03}_{-0.02}$	...	$6.18^{+0.04}_{-0.04}$	1.32 | 891	100.0%
	$2.87^{+0.07}_{-0.07}$	$1.85^{+0.02}_{-0.02}$	...	$7.69^{+0.06}_{-0.06}$	...	1.18 | 891	100.0%
	$5.0^{+0.4}_{-0.4}$	$1.99^{+0.03}_{-0.03}$	$0.12^{+0.01}_{-0.00}$	$8.7^{+0.2}_{-0.2}$	25^{+14}_{-9}	1.12 | 889	99.2%
			IC 342 X-6				
0093640901	$3.4^{+0.3}_{-0.3}$	...	$2.0^{+0.2}_{-0.1}$	...	$4.9^{+0.2}_{-0.2}$	1.14 | 179	89.9%
	$5.7^{+0.6}_{-0.5}$	$1.65^{+0.09}_{-0.08}$	...	$5.9^{+0.2}_{-0.2}$	...	0.88 | 179	13.4%
2916	$3.1^{+0.5}_{-0.1}$	...	$1.9^{+0.2}_{-0.2}$	...	$5.3^{+0.3}_{-0.3}$	1.16 | 80	84.1%
	$5.4^{+0.7}_{-0.7}$	$1.63^{+0.13}_{-0.12}$	...	$6.5^{+0.2}_{-0.2}$	...	0.79 | 80	8.3%
2917	$3.6^{+0.5}_{-0.5}$	...	$1.8^{+0.2}_{-0.2}$	...	$5.2^{+0.3}_{-0.2}$	1.51 | 86	99.8%
	$6.2^{+0.8}_{-0.8}$	$1.70^{+0.13}_{-0.13}$	...	$6.7^{+0.3}_{-0.2}$	...	1.21 | 86	91.1%
0206890101	$4.8^{+0.2}_{-0.15}$	...	$1.58^{+0.04}_{-0.04}$	...	$11.28^{+0.06}_{-0.05}$	1.22 | 798	100.0%
	$8.2^{+0.3}_{-0.3}$	$1.99^{+0.04}_{-0.03}$	...	$16.0^{+0.4}_{-0.4}$	...	0.97 | 798	26.5%
	$10.7^{+1.4}_{-1.5}$	$2.10^{+0.07}_{-0.07}$	$0.14^{+0.02}_{-0.02}$	18^{+1}_{-1}	42^{+62}_{-29}	0.96 | 796	21.3%
0206890201	$3.6^{+0.2}_{-0.2}$	...	$1.75^{+0.06}_{-0.06}$	...	$5.45^{+0.08}_{-0.08}$	1.47 | 524	100.0%
	$6.3^{+0.3}_{-0.3}$	$1.81^{+0.05}_{-0.05}$	...	$7.03^{+0.16}_{-0.15}$	...	1.01 | 524	58.2%
	$7.4^{+1.1}_{-0.8}$	$1.70^{+0.09}_{-0.10}$	$0.29^{+0.10}_{-0.06}$	$6.7^{+0.4}_{-0.4}$	$2.2^{+2.9}_{-1.1}$	0.98 | 522	36.4%
0206890401	$4.9^{+0.3}_{-0.2}$	...	$1.74^{+0.07}_{-0.06}$	...	$14.9^{+0.2}_{-0.2}$	1.23 | 429	99.9%
	$8.3^{+0.4}_{-0.4}$	$1.87^{+0.05}_{-0.05}$	...	$19.8^{+0.7}_{-0.6}$	...	1.07 | 429	84.5%
	$11.0^{+1.8}_{-1.8}$	$2.00^{+0.09}_{-0.09}$	$0.13^{+0.02}_{-0.02}$	22^{+2}_{-2}	105^{+198}_{-76}	1.05 | 427	78.4%
			Holmberg II X-1				
0112520601	$1.7^{+0.1}_{-0.1}$	$2.71^{+0.04}_{-0.04}$	...	$25.0^{+0.7}_{-0.7}$	...	1.03 | 652	69.6%
	$1.4^{+0.4}_{-0.3}$	$2.5^{+0.2}_{-0.2}$	$0.30^{+0.06}_{-0.10}$	11^{+2}_{-2}	$3.0^{+1.0}_{-1.0}$	1.00 | 650	48.5%
0112520701	$1.14^{+0.1}_{-0.1}$	$2.42^{+0.05}_{-0.05}$	...	$19.2^{+0.6}_{-0.6}$	...	1.03 | 503	68.7%
	$1.2^{+0.3}_{-0.2}$	$2.2^{+0.1}_{-0.1}$	$0.22^{+0.05}_{-0.04}$	$9.4^{+0.7}_{-0.8}$	$3.6^{+2.1}_{-1.2}$	0.97 | 501	31.8%
0112520901	$1.3^{+0.2}_{-0.2}$	$3.0^{+0.1}_{-0.1}$	...	$5.4^{+0.5}_{-0.4}$	...	1.08 | 202	79.9%
	$1.5^{+0.6}_{-0.4}$	$2.8^{+0.2}_{-0.2}$	$0.16^{+0.07}_{-0.04}$	$2.6^{+0.5}_{-0.5}$	$1.9^{+4.5}_{-1.3}$	1.06 | 200	71.8%
0200470101	$1.70^{+0.03}_{-0.03}$	$2.72^{+0.01}_{-0.01}$	...	$26.4^{+0.3}_{-0.3}$	...	1.25 | 1338	100.0%
	$1.62^{+0.08}_{-0.08}$	$2.55^{+0.03}_{-0.04}$	$0.24^{+0.02}_{-0.02}$	$12.7^{+0.5}_{-0.5}$	$3.3^{+0.5}_{-0.4}$	1.12 | 1336	99.9%
			Holmberg IX X-1				
0112521001	$1.5^{+0.1}_{-0.1}$	$1.79^{+0.03}_{-0.03}$	...	$11.5^{+0.1}_{-0.1}$	...	1.06 | 813	87.4%
	$1.8^{+0.3}_{-0.2}$	$1.67^{+0.05}_{-0.06}$	$0.27^{+0.06}_{-0.04}$	$10.9^{+0.3}_{-0.4}$	$2.0^{+1.0}_{-0.6}$	1.02 | 811	63.0%
0112521101	$1.8^{+0.1}_{-0.1}$	$1.85^{+0.03}_{-0.03}$	...	$13.8^{+0.2}_{-0.2}$	...	0.97 | 908	28.3%
	$2.0^{+0.3}_{-0.2}$	$1.77^{+0.05}_{-0.06}$	$0.26^{+0.07}_{-0.05}$	$13.3^{+0.4}_{-0.5}$	$1.9^{+1.3}_{-0.7}$	0.95 | 906	15.1%
3786	$1.4^{+0.1}_{-0.1}$	$1.73^{+0.05}_{-0.04}$	...	$11.76^{+0.06}_{-0.05}$	...	1.16 | 249	95.9%
	$1.8^{+0.5}_{-0.4}$	$1.61^{+0.09}_{-0.12}$	$0.25^{+0.10}_{-0.06}$	$11.5^{+0.4}_{-0.5}$	$1.7^{+1.5}_{-0.7}$	1.09 | 247	84.0%
3787	$2.1^{+0.1}_{-0.1}$	$1.92^{+0.04}_{-0.04}$	...	$16.6^{+0.2}_{-0.2}$	...	1.12 | 259	90.6%
3788	$1.5^{+0.15}_{-0.15}$	$1.70^{+0.05}_{-0.05}$	...	$10.27^{+0.07}_{-0.06}$	...	1.14 | 215	92.5%
	$2.2^{+0.7}_{-0.5}$	$1.55^{+0.11}_{-0.13}$	$0.23^{+0.08}_{-0.05}$	$10.0^{+0.4}_{-0.5}$	$2.3^{+2.1}_{-0.9}$	1.02 | 213	60.4%
0200980101	$1.07^{+0.03}_{-0.03}$	$1.61^{+0.01}_{-0.01}$	...	$9.30^{+0.02}_{-0.02}$	...	1.46 | 2088	100.0%
	$1.8^{+0.1}_{-0.1}$	$1.48^{+0.02}_{-0.02}$	$0.24^{+0.01}_{-0.01}$	$9.04^{+0.08}_{-0.08}$	$2.7^{+0.4}_{-0.3}$	1.12 | 2086	100.0%
			NGC 5204 X-1				
0142770101	$0.5^{+0.1}_{-0.1}$	$2.05^{+0.05}_{-0.05}$	...	$3.68^{+0.07}_{-0.07}$	...	0.98 | 501	36.5%
	$0.7^{+0.3}_{-0.2}$	$1.92^{+0.08}_{-0.08}$	$0.23^{+0.06}_{-0.04}$	$3.4^{+0.2}_{-0.2}$	$0.9^{+0.6}_{-0.3}$	0.94 | 499	16.2%
0142770301	$1.0^{+0.2}_{-0.2}$	$2.33^{+0.09}_{-0.09}$	...	$5.3^{+0.3}_{-0.2}$	...	1.01 | 208	56.0%
	$1.7^{+0.8}_{-0.6}$	$2.15^{+0.14}_{-0.15}$	$0.17^{+0.05}_{-0.03}$	$4.9^{+0.5}_{-0.5}$	$4.9^{+7.5}_{-2.7}$	0.90 | 206	14.9%
0150650301	$1.2^{+0.2}_{-0.2}$	$2.48^{+0.08}_{-0.08}$	...	$6.3^{+0.3}_{-0.3}$	...	1.01 | 295	56.7%
	$1.2^{+0.6}_{-0.6}$	$2.2^{+0.2}_{-0.3}$	$0.25^{+0.11}_{-0.08}$	$5.2^{+0.8}_{-1.2}$	$1.9^{+2.0}_{-0.8}$	0.97 | 293	35.5%
3933	$1.6^{+0.15}_{-0.15}$	$2.94^{+0.08}_{-0.08}$	...	$3.8^{+0.2}_{-0.2}$	...	1.64 | 147	100.0%
	$1.7^{+0.3}_{-0.3}$	$2.67^{+0.13}_{-0.14}$	$0.19^{+0.04}_{-0.03}$	$3.0^{+0.4}_{-0.4}$	$1.4^{+0.8}_{-0.5}$	1.45 | 145	100.0%

Continued on next page…

Table A1 – Continued

Obs.ID	$N_{\rm H}$ [a]	Γ [b]	$T_{\rm in}$ [c]	$L_{\rm power-law}$ [d]	$L_{\rm diskbb}$ [e]	$\chi^2_{\rm red}$ | d.o.f. [f]	$P_{\rm rej}$ [g]
0405690101	$1.6^{+0.1}_{-0.1}$	$2.73^{+0.05}_{-0.05}$	...	$9.0^{+0.3}_{-0.3}$	...	1.07 | 584	89.6%
	$1.5^{+0.2}_{-0.2}$	$2.6^{+0.1}_{-0.1}$	$0.23^{+0.07}_{-0.06}$	$8.0^{+0.7}_{-0.9}$	$1.7^{+1.4}_{-0.8}$	1.06 | 582	85.1%
0405690201	$1.52^{+0.07}_{-0.07}$	$2.62^{+0.03}_{-0.03}$	...	$7.5^{+0.2}_{-0.2}$	...	1.15 | 818	99.8%
	$1.25^{+0.15}_{-0.15}$	$2.34^{+0.08}_{-0.09}$	$0.29^{+0.03}_{-0.03}$	$5.8^{+0.5}_{-0.5}$	$1.8^{+0.3}_{-0.4}$	1.08 | 816	94.2%
0405690501	$0.84^{+0.08}_{-0.08}$	$2.27^{+0.04}_{-0.04}$	...	$4.7^{+0.1}_{-0.1}$	...	1.09 | 669	94.2%
	$0.7^{+0.2}_{-0.2}$	$1.9^{+0.1}_{-0.1}$	$0.28^{+0.03}_{-0.03}$	$3.7^{+0.2}_{-0.3}$	$1.7^{+0.3}_{-0.3}$	0.92 | 667	7.5%
			NGC 5408 X-1				
0112290501	$1.3^{+0.2}_{-0.2}$	$3.5^{+0.1}_{-0.1}$	...	$10.1^{+1.1}_{-1.0}$	...	1.28 | 270	99.9%
	$1.0^{+0.4}_{-0.4}$	$2.7^{+0.2}_{-0.2}$	$0.18^{+0.03}_{-0.02}$	$4.9^{+1.1}_{-1.0}$	$8.8^{+5.0}_{-2.5}$	1.06 | 268	75.9%
0112290601	$1.4^{+0.2}_{-0.2}$	$3.5^{+0.1}_{-0.1}$	...	$10.1^{+1.1}_{-1.0}$	...	1.09 | 278	85.6%
	$0.7^{+0.4}_{-0.3}$	$2.5^{+0.3}_{-0.3}$	$0.22^{+0.03}_{-0.03}$	$3.9^{+1.1}_{-0.9}$	$6.7^{+2.1}_{-1.4}$	0.89 | 276	8.5%
0112290701	$0.9^{+0.3}_{-0.2}$	$3.21^{+0.16}_{-0.15}$	...	$8.7^{+1.1}_{-0.9}$	...	1.13 | 141	86.9%
	$0.8^{+0.6}_{-0.5}$	$2.7^{+0.3}_{-0.3}$	$0.18^{+0.05}_{-0.04}$	$5.5^{+1.5}_{-1.4}$	$6.8^{+7.7}_{-2.9}$	0.99 | 139	49.2%
0112291201	$1.2^{+0.3}_{-0.3}$	$3.00^{+0.17}_{-0.16}$	...	$6.1^{+0.8}_{-0.6}$	...	1.35 | 143	99.6%
	$1.2^{+0.7}_{-0.6}$	$2.2^{+0.3}_{-0.3}$	$0.19^{+0.05}_{-0.04}$	$3.4^{+0.8}_{-0.7}$	$6.2^{+5.6}_{-2.2}$	1.05 | 141	66.2%
0302900101	$1.35^{+0.1}_{-0.1}$	$2.66^{+0.04}_{-0.04}$	$0.17^{+0.01}_{-0.01}$	$4.8^{+0.2}_{-0.2}$	$8.4^{+1.1}_{-0.9}$	1.30 | 978	100.0%
			NGC 6946 X-6				
1043	$2.2^{+0.2}_{-0.2}$	$2.5^{+0.1}_{-0.1}$	...	$4.7^{+0.2}_{-0.2}$	...	1.57 | 165	100.0%
	$3.7^{+0.6}_{-0.6}$	$2.2^{+0.1}_{-0.1}$	$0.16^{+0.02}_{-0.02}$	$4.1^{+0.4}_{-0.3}$	$7.1^{+4.9}_{-2.8}$	0.95 | 163	33.4%
4404	$2.3^{+0.3}_{-0.2}$	$2.4^{+0.1}_{-0.1}$	...	$4.3^{+0.2}_{-0.2}$	...	1.59 | 117	100.0%
	$4.1^{+1.0}_{-0.9}$	$2.2^{+0.2}_{-0.2}$	$0.16^{+0.03}_{-0.02}$	$3.8^{+0.5}_{-0.4}$	$7.7^{+9.2}_{-3.9}$	1.12 | 115	82.6%
0200670301	$2.6^{+0.3}_{-0.3}$	$2.8^{+0.1}_{-0.1}$	...	$5.2^{+0.5}_{-0.4}$	...	1.19 | 166	95.2%
	$3.1^{+0.9}_{-0.7}$	$2.4^{+0.2}_{-0.2}$	$0.20^{+0.05}_{-0.04}$	$3.7^{+0.8}_{-0.7}$	$5.8^{+7.5}_{-2.6}$	0.98 | 164	43.7%
4631	$2.4^{+0.3}_{-0.3}$	$2.7^{+0.2}_{-0.1}$	...	$4.0^{+0.4}_{-0.3}$	...	1.58 | 100	100.0%
	$4.2^{+1.2}_{-1.0}$	$2.3^{+0.2}_{-0.2}$	$0.16^{+0.04}_{-0.03}$	$3.3^{+0.6}_{-0.5}$	$8.3^{+12}_{-4.5}$	1.11 | 98	79.2%
4632	$2.2^{+0.3}_{-0.3}$	$2.5^{+0.1}_{-0.1}$	...	$4.4^{+0.3}_{-0.3}$	...	1.94 | 102	100.0%
	$4.9^{+1.1}_{-1.0}$	$2.3^{+0.2}_{-0.2}$	$0.14^{+0.03}_{-0.02}$	$4.0^{+0.6}_{-0.5}$	17^{+23}_{-9}	1.36 | 100	99.0%
4633	$2.2^{+0.3}_{-0.3}$	$2.6^{+0.1}_{-0.1}$	...	$4.3^{+0.3}_{-0.3}$	...	1.71 | 107	100.0%
	$4.6^{+1.1}_{-1.0}$	$2.2^{+0.2}_{-0.2}$	$0.14^{+0.03}_{-0.02}$	$3.8^{+0.6}_{-0.5}$	14^{+19}_{-7}	1.05 | 105	66.0%
0401360301	$2.5^{+0.5}_{-0.5}$	$2.7^{+0.2}_{-0.2}$	...	$5.8^{+1.1}_{-0.8}$	...	1.28 | 62	93.2%
	$3.0^{+1.5}_{-1.2}$	$2.3^{+0.4}_{-0.6}$	$0.21^{+0.11}_{-0.07}$	$4.2^{+1.6}_{-1.4}$	$5.6^{+22}_{-3.7}$	1.19 | 60	84.7%

[a] Hydrogen column density in units 10^{21} cm^{-2}.
[b] Photon index.
[c] Inner disk temperature of the DISKBB component in units of keV.
[d] Power-law model luminosity in 0.4–10 keV band in units of 10^{39} erg s^{-1}.
[e] DISKBB model bolometric luminosity (computed in 0.01–50 keV band) in units of 10^{39} erg s^{-1}.
[f] Reduced χ^2 and the degrees of freedom.
[g] Rejection probability.